Microstructure and point defects in CdTe nanowires for photovoltaic applications

B. L. Williams[1*], D.P. Halliday[2], B. G. Mendis[2] and K. Durose[1]

[1]Stephenson Institute for Renewable Energy, Liverpool University, Liverpool, L69 7ZF, UK

[2]Department of Physics, Durham University, South Road, Durham, DH1 3LE, UK

*Corresponding author; b.l.williams@liverpool.ac.uk (Tel: +44 (0)151 795 9050)

Receipt date: 19/12/2012

PACS indexing codes: 78.67.Uh, 78.66.Hf, 78.55.Et, 88.40.jm

Abstract

Defects in Au-catalysed CdTe nanowires VLS-grown on polycrystalline underlayers have been critically evaluated. Their low-temperature photoluminescence spectra were dominated by excitonic emission with rarely observed above-gap emission also being recorded. While acceptor bound exciton lines due to monovalent metallic impurities (Ag, Cu or Na) were seen, only deeper, donor acceptor pair emission could be attributed to the Au contamination that is expected from the catalyst. Annealing under nitrogen acted to enhance the single crystal-like PL emission, whilst oxidising and reducing anneals of the type that are used in solar cell device processing caused it to degrade. The incidence of stacking faults, polytypes and twins was related only to the growth axes of the wires (<111> 50%, <112> 30% and <110> 20%), and was not influenced by annealing. The potential electrical activity of the point and extended defects, and the suitability of these nanowire materials (including processing steps) for solar cell applications, is discussed. Overall they have quality that is superior to that of thin polycrystalline films, although questions remain about recombination due to Au.

1. Introduction

Both microstructural and point defects have profound effects on the conversion efficiencies of photovoltaic (PV) devices. In the case of grain boundaries, recombination loss - leading to reduction in the open circuit voltage and short circuit current - is very significant [1]. Even when such boundaries are passivated to electrical recombination [2], they may nevertheless contribute to the series resistance of the devices, that acts to reduce their fill factor, as has been shown for CdTe solar cells [3]. Moreover, the electrical activity of grain boundaries depends on their crystallographic make up [4], with pure $\Sigma = 3$ coherent twin boundaries being inactive, and all others being active in zinc blende semiconductors. The influence of point defects (including substitutional, vacancy and complex types) is similarly complicated: point defects are responsible for both the shallow levels that (beneficially) control the conductivity type of the semiconductors, and also for the compensating and deep level behaviour that is deleterious to solar cell performance. Indeed, for the case of CdTe, the current transport is usually recombination dominated, with the diode factor of the junctions being ≥ 2 [5], implying that interface or else deep level states in the bulk are dominant. Moreover, point defect clouds may interact with extended defects, leading to non-uniform electrical conductivity and recombination behaviour [6, 7], for example near to grain boundaries where gettering takes place.

The literature contains many accounts of the various processing steps used for CdTe solar cells. These include annealing of the layers (in air and with chlorides) that is considered to have beneficial effects on both microstructure (grain growth, recrystallization) and point defects (stabilisation and control of V_{Cd} populations through the A-centre, V_{Cd}-Cl_{Te}). The challenges presented by microstructure and point defects are considered to be ubiquitous in state of the art thin film polycrystalline CdTe PV devices. Accordingly, since 1992 [8], technological progress in achieving increases in efficiency has been slow, with the most recent record being just 1.5% higher than the 15.8% record of twenty years ago [9]. Research on other device concepts for CdTe PV is therefore timely, including that on nanowire devices.

In this work we explore the microstructure and point defects present in CdTe nanowires (NWs) - in order to assess their potential for use in PV devices. The NWs were grown on continuous thin films of CdTe in a geometry that is appropriate for use in PV device architectures. We demonstrate that such NWs have point defect

and microstructural behaviour that is very different from that of polycrystalline thin films, and is of a quality similar to that in single crystals. The appropriateness of the NWs for PV applications is discussed.

Recently there has been considerable interest in the development of NW based PV devices, particularly with the aim of overcoming the technological limitations of both amorphous and crystalline thin film silicon. The benefits of the approach are considered to be a) increased light trapping from low volumes of material compared to thin films [10] and b) the separation of the processes of optical absorption and of carrier collection i.e. with absorption taking place as light travels down the length of a NW and carrier collection taking place over its width [11, 12], this being postulated to minimise recombination loss provided the NW radius is smaller than the average carrier diffusion length. For the case of CdTe NW PV, modelling has indicated that 20% efficiency should be achievable [13], whereas 6% has been reached in practice, this being demonstrated using CdS nanopillars coated with CdTe [14]. At the present time there are no published reports of NW PV devices based on CdTe NWs, and only one report [15] of the growth of CdTe NWs on conductive substrates by the Au-catalysed vapour – liquid – solid growth mechanism, this being followed up with a modelling study [16]. Despite the lack of experimental evidence so far, the performance of NW CdTe cells may nevertheless be expected to be influenced by both the populations of microstructural and point defects within the CdTe NWs as explained above: that is the motivation for their study in this work. Both as-grown and annealed NWs are analysed, with low-temperature photoluminescence (PL), SEM and TEM being the principal methods used.

2. Experimental Procedure

The procedure for the growth of the CdTe NW arrays was as follows: First, continuous films of polycrystalline CdTe (1 μm thick) were deposited onto soda-lime glass by RF magnetron sputtering (5N target, Ar pressure 10 mTorr, 70 W, substrate temperature 250°C). A gold catalyst droplet array was then generated by thermally evaporating a 5 nm Au film onto this CdTe buffer layer and then annealing at 360°C for 30 mins under 10 Torr N_2. The gold supplied by Advent was 99.5% pure; the manufacturer giving a typical impurity analysis in ppm of Ag – 80, Cu – 20, Pt – 20, Fe – 3, Mg – 1, and Si – 1. The wires themselves were formed by subliming 5N-pure CdTe (in a 'close space sublimation' apparatus – CSS) for 15 mins with the source being held at 550°C,

the sample at 500°C and under 10 Torr of N_2. The process generates dense arrays of NWs as is shown schematically in figure 1a. Further details of the growth and a discussion of the growth mechanism may be found in Ref. 15. The NW arrays were subsequently annealed on their substrates for 30 minutes in the following environments: a) as-grown control, b)100 Torr N_2 at 400°C, c) air at 400°C, d)10 Torr O_2 + 90 Torr N_2 400°C, e) 100 Torr N_2 at 500°C and f) 10 Torr H_2 + 90 Torr N_2 at 400°C. These annealing conditions have been chosen as they are similar to those that have been used to improve the microstructure of CdTe in thin-film solar cells [17, 18].

Low temperature PL spectra were excited using the 514 nm line of an argon ion laser (spot size, d = 1 mm) which was highly linearly polarised in the vertical by use of a Brewster window, although with the beam being reflected by four mirrors there will be some degradation of the polarisation. The beam was incident at an angle of 20° to the normal, with the samples being held at 4K in a closed-cycle He cryostat. PL spectra were recorded both from the NW arrays on their substrates and from NWs that had been removed by pressing the samples onto clean Si (111) wafers, the latter being more informative (see below). Electron microscope imaging and structural characterisation were carried out using a Hitachi SU-70 FEG SEM and a JEOL 2100F FEG TEM.

3. Results and Discussion

A backscattered SEM image of a typical CdTe NW array is shown in figure 1b. The wires were up to 20 μm long and had diameters in the range 100 – 300 nm – this not being small enough for quantum confinement to become an important consideration. Nevertheless the NW radii are smaller than the reported carrier diffusion lengths for CdTe [19] and are hence suitable for PV applications. Their densities – estimated from SEM images – were in the range $10^7 – 10^8$ cm^{-2}. An evaluation of the point defects and microstructure now follows.

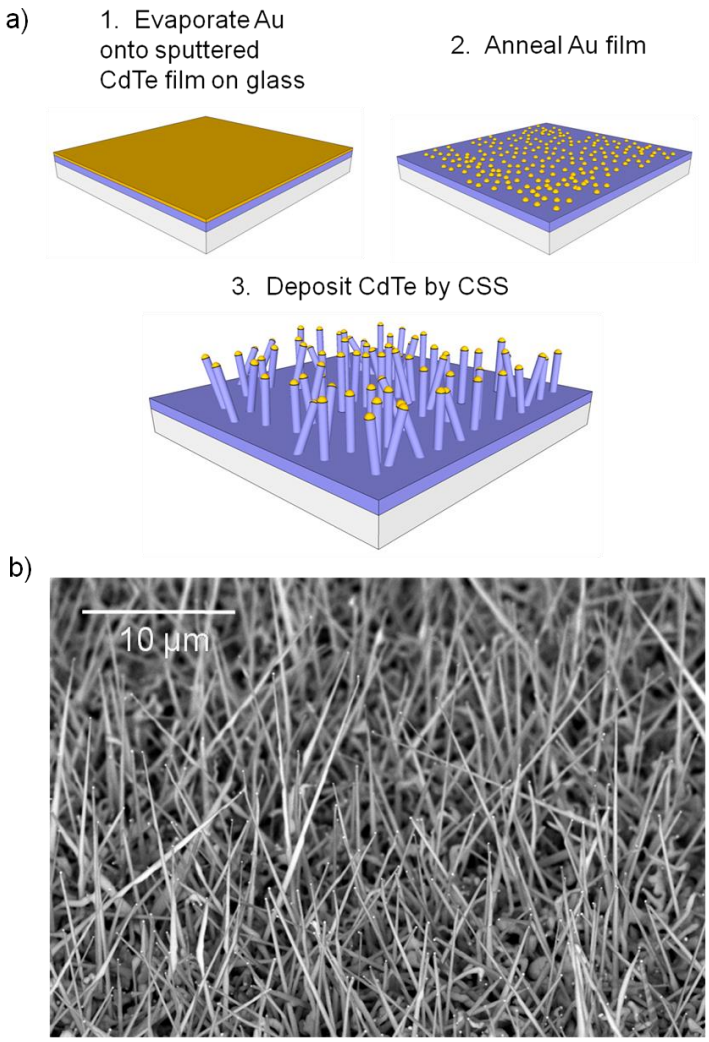

Figure 1: (a) Schematic diagram of the 'metamorphic' growth of CdTe NWs from an array of Au catalyst droplets resting on continuous CdTe film. (b) Back-scattered electron image of a typical CdTe NW array. Au catalyst droplets appear on the NW tips as bright contrast due to their atomic number.

3.1. Photoluminescence from CdTe control films and nanowire arrays on their substrates

Figure 2 shows a comparison between the PL from - a) a control film of polycrystalline CdTe, b) an array of NWs on their substrate, and c) a group of NWs that have been isolated by removing them from their substrate onto a clean Si wafer. Si does not emit any luminescence in the region we are considering here.

The spectra from both the films and the NW arrays on their films differ greatly from those from the isolated NWs: The former both comprise a broad donor-acceptor-pair (DAP) luminescence band (~1.35 – 1.5 eV) having no fine structure, and little or no near-edge emission. Indeed this is typical for a polycrystalline semiconductor film [20-22] in which it is generally supposed that the fields associated with grain boundaries and dangling bonds or impurity states cause the loss of fine structure and the quenching of excitonic emission. On the contrary, for the case of the isolated NWs, the spectra contain both near-edge peaks (~1.55 - 1.6 eV) and donor-acceptor-pair (DAP) peaks (~1.35 – 1.5 eV) that show fine structure. This is more typical of PL from single crystal materials, in which the excitonic emission is relatively strong compared to the DAP emission. Indeed, the ratio of excitonic to DAP emission is used as a measure of the 'quality' of CdTe, this being influenced both by microstructure and the populations of point defects participating in the transitions [23]. It may be inferred that for the case of NWs on a polycrystalline CdTe layer, the layer dominates the PL emission, considering the similarity of the spectrum to that of just the CdTe film. The presence of the NWs in this configuration merely causes inhomogenous broadening of the spectra as there is a range of NW diameters. However, for the case of isolated NWs the wires themselves have PL emission that is representative of high quality single crystals. We do not attribute any differences in the PL spectra between intact NWs and isolated NWs to differences in their orientation – intact NWs being oriented at a range of angles to the substrate, and isolated NWs lying flat on the substrate – as since these particular NWs are zinc-blende (see Section 3.3.4), their optical properties are isotropic.

For the purposes of this work, the removal of the wires from their substrates clearly gives spectra that are unique to the wires, and which give the opportunity for the further spectral analysis and line identification that are presented in the next section. Incidentally, for normalizing of these spectra, the intensity of the emission from the isolated NWs had to be multiplied by a factor of ~ 5, although it must be noted that the surface coverage of isolated NWs on the Si substrate in this case was only 20 ± 5 % (estimated using the *Image Tool*™ analysis software), i.e. ~ the semiconductor excitation volume was much lower than for the films and for the NW arrays on films.

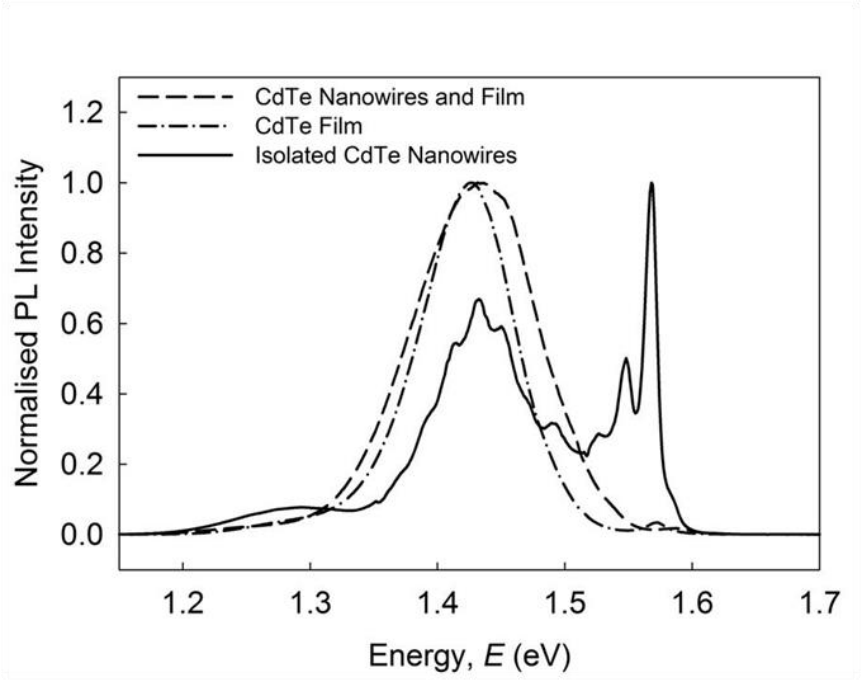

Figure 2: Comparison of PL spectra (4K) from CdTe: a) dash/dotted line – control film of sputtered CdTe, b) dashed line – NW array on a polycrystalline CdTe film, and c) NWs that had been isolated by removal from their substrate onto a clean Si wafer. The latter shows strong excitonic emission and fine structure in the peaks that is discussed in the text. Table 1 provides a summary of the main luminescence data from the NW samples, while table 2 gives lists the data from the literature cited in the discussion.

3.2. Photoluminescence of isolated nanowires (as-grown samples)

In this section the origin of the peaks in the PL spectra in Figs 2, 3 and 4a and summarised in table 1 are described and discussed with reference to both our own mechanistic studies and the literature. Since the NWs might be expected to be contaminated by the Au catalyst (and possibly its minor impurities) we have given special consideration to the contributions to the luminescence from Au, Cu, Ag and Na, with the relevant literature reports being shown in table 2.

Firstly, the excitonic region with peak energies greater than 1.5 eV: High energy peaks in this region are reported to be associated with excitons bound to neutral acceptors, A^0X, and their phonon replicas. The most

intense lines in this region in these samples were at 1.589, 1.569 and 1.548 eV (figure 3 inset), which are indeed separated by the LO phonon energy (20 – 21 meV) The relation between the PL intensity *I* and the incident light *L*, $I \propto L^k$ often holds for PL experiments, with the value of *k* being a useful diagnostic tool for identifying the origin of transitions. Excitonic transitions have $k > 1$, while all others, including DAP for example, have $k < 1$, as discussed by Schmidt [24]. For the case of the 1.569 and 1.548 eV lines, the exponents were 1.27 and 1.13 respectively (figure 3 main), which is consistent with them being excitonic transitions. Moreover, as expected for excitonic transitions, no change to the peak position of these features was observed as the excitation intensity was increased. It is noticeable that the most intense line in this phonon replica series is the first phonon replica (A^0X-1LO) peak at 1.569 eV – and while this is uncommon there are reports of it for CdTe [25], ZnO [26-28] and GaN [29]. The intensities of phonon replica peaks is normally attributed to the strength of the electron-phonon coupling arising from the Frölich potential, and this is usually strong for CdTe. Indeed, for these peaks the Huang-Rhys coupling parameter was estimated as $S = 2.0$. However the fit of the peak intensity series to the Poisson envelope was not good, with the first phonon replica being more, and the higher orders less intense than expected. Since there is no such discrepancy for the DAP phonon replica series described later in this work, we conclude that the luminescence is not perturbed from the bulk on account of presence of surface defects as has been postulated elsewhere [27, 28]. Instead we speculate that there is an overlap of the A^0X-1LO peak with an unidentified emission line - and the fact that the (combined) line does not have a pure Gaussian shape supports this possibility. Magnea [30] summarises the following principal bound exciton PL line energies (recorded at 1.8K): Ag^0X - 1.58848, Cu^0X 1.58956, Na^0X – 1.58916 and Au^0X – 1.57606 eV. It is clear from this that the Au^0X line is absent from the NW spectra whereas it is reported as present for diffused [31] and implanted [32] samples. There was also no match to the positions of Au^0X phonon replica lines. However, the luminescence is consistent with A^0X emission from either Ag, Cu or Na which may be present from impurities in the Au (Ag 80, Cu 20 ppm) or from the glass (Na). Since the lines lie within 0.00112 eV of one another and within 0.0006 eV of the peak we measured, this experiment cannot distinguish between them. We have therefore assigned the line at 1.589 eV to being A^0X (A being possibly Ag, Cu or Na), and the 1.569 and 1.548 eV lines as its phonon replicas (as shown in table 1). From the levels of Ag and Cu in the Au, and the fact that Na would have to diffuse from

the glass, we consider the most likely acceptor to be Ag followed by Cu and then Na. Given the lack of near edge Au luminescence, we also looked for matches to other Au-related lines in this region, these being the series of three lines assigned to the neutral complex $Au_{Cd} - Au_i$ by Molva [31], as shown in table 2, and having energies 1.57210, 1.53850 and 1.52668 eV. However, there is no match to the first (1.57210 eV), and we considered it unlikely that the second two (1.53850 and 1.52668 eV) were hidden under the lines at 1.539 and 1.529 eV for the following reasons: a) Molva reports that the three complex lines *only* appear alongside the Au^0X line, which is missing here, and b) Molva reports that all three complex lines appear together, but the first is clearly missing from our spectra. Overall, there is no evidence of Au related near-edge emission from these samples, although deeper emission is reported below. The reader is referred to subsection C.i for a discussion of the above-gap emission seen in some of the heat-treated samples.

Secondly, the series of seven peaks and shoulders in the broad feature that is seen in Figs 2 and 4 are considered: Such features are widely seen in CdTe and are ascribed to donor-acceptor pair (DAP) transitions and their phonon replicas. Indeed, like the near-edge luminescence, emission for these samples is reminiscent of the spectra from single crystal samples. The Huang-Rhys coupling parameter for the series was measured as S = 2.5, indicating strong-electron phonon coupling (there was a good fit between the Poissonian envelope and the intensities). This S-value is typical for the A-centre [Cl_{Te}-V_{Cd}] in CdTe, although in these samples there were no intentionally introduced halogens. The exponent values of $k \cong 0.75$ for the peaks in the series (table 1) are also evidence that this is DAP emission. Moreover, the blue shift of this band (~ 6 meV), observed upon increasing the excitation intensity in the range 60 – 2000 mW/cm^2, is a common feature of DAP transitions as the energy of emitted photons is dependent on the coulomb potential, which is inversely proportional to the spatial separation of donors and acceptors. Greater excitation intensity gives an increased photo-excited carrier concentration leading to increased free carrier screening so that more closely spaced DA pairs dominate.

the peak position observed blue shift of the peaks with increasing laser intensity – this blue shift is a result of the DAP emission energy being dependent on the coulombic separation term, However, since the DAP spectra from CdTe is usually at very similar energies, even for material doped with a wide range of impurities, it is only

possible to infer its origin from knowledge of the impurity content of the particular samples. Hence here we must infer the participating acceptor to be Ag, Cu or Na in order of decreasing probability (as discussed above).

Thirdly, we discuss the broad and weak peak on the low energy side of the spectrum in figure 2 which was modelled as a single peak at 1.287 eV in our de-convolution: It has a *k* value of 0.5, which is consistent with DAP emission. This peak is also consistent with reports of Au-related DAP luminescence: Molva recorded a phonon replica series for CdTe:Au with the peak of the envelope being in the range 1.275 – 1.284 eV; Hamann's implanted sample had a broad peak at 1.267 and de Nobel's [33] work at 77K had a peak at 1.27 eV. We also considered the possibility that this line is oxygen related (since results presented later involve air annealing). However, since the deep oxygen emission is generally at a lower energy, as shown by Vatavu [34] for example, we assigned the 1.287 eV emission to Au.

Table 1. Photoluminescence bands excited from CdTe nanowires in this work and their assignments.

Region	Energy (eV)	*k*	Notes	Assignment	Origin
Near Edge	1.614		Above-gap emission seen in only a few samples	FE or A^0X with anti-Stokes process	Ag, Cu or Na
	1.589		Strong line S = 1.8 (for A^0X series)	A^0X	Ag, Cu or Na
	1.569	1.27	Strong line	A^0X – 1LO (+ unassigned feature)	Ag, Cu or Na
	1.548	1.13	Weaker line. Lower k value than normal for excitonic, but > 1, not eA^0	A^0X – 2LO	Ag, Cu or Na
	1.539	-	Weak shoulder of 1.548 eV peak	Not assigned	
	1.529	-	Weak shoulder of 1.548 eV peak	A^0X – 3LO ?	Ag, Cu or Na
DAP region	1.491	0.76	S = 2.5 (for DAP series)	DAP	
	1.472	0.75		DAP – 1LO	
	1.452	0.77		DAP – 2LO	
	1.432	0.74	Strongest peak in series	DAP – 3LO	
	1.412	0.73		DAP – 4LO	
	1.392	-		DAP – 5LO	
	1.372	-		DAP – 6LO	
Deep region	1.287	0.5	Weak and broad	DAP	Au

Table 2. Literature reports of photoluminescence lines due to Au, Cu and Na. Values marked * are the positions of phonon replica lines estimated using an LO phonon energy of 21.2 meV [30], and are not shown in the spectra in the references given. They are included for comparison with the lines observed in this work.

(Au) Molva [23] (eV)	**(Au) Hamman [24] (eV)**	**(Au) de Nobel [25] (eV)**	**(Cu) Hamman [24] (eV)**	**(Cu) Magnea [22] (eV)**	**(Ag) Magnea [22] (eV)**	**(Na) Magnea [22] (eV)**
1.57606 Au^0X	1.5761 Au^0X		1.5896 Cu^0X	1.58956 Cu^0X	1.58848 Ag^0X	1.58916 Na^0X
1.55486 Au^0X – 1LO				1.56836 Cu^0X – 1LO	1.56728* Ag^0X-1LO	1.56796 Na^0X-1LO
1.53366 Au^0X – 2LO				1.54716* Cu^0X – 2LO	1.54608* Ag^0X-2LO	1.54676* Na^0X-2LO
1.57210 'C_1^{Au}' Au_{Cd} – Au_i neutral				1.52596* Cu^0X – 3LO	1.52488* Ag^0X-3LO	1.52556* Na^0X-3LO
1.53850 'C_2^{Au}' Au_{Cd} – Au_i neutral				1.50476* Cu^0X – 4LO	1.50368* Ag^0X-4LO	1.50436* Na^0X-4LO
1.52688 'C_3^{Au}' Au_{Cd} – Au_i neutral						
DAP series of 6 peaks centred at 1.28	DAP series centred at 1.267	1.287				

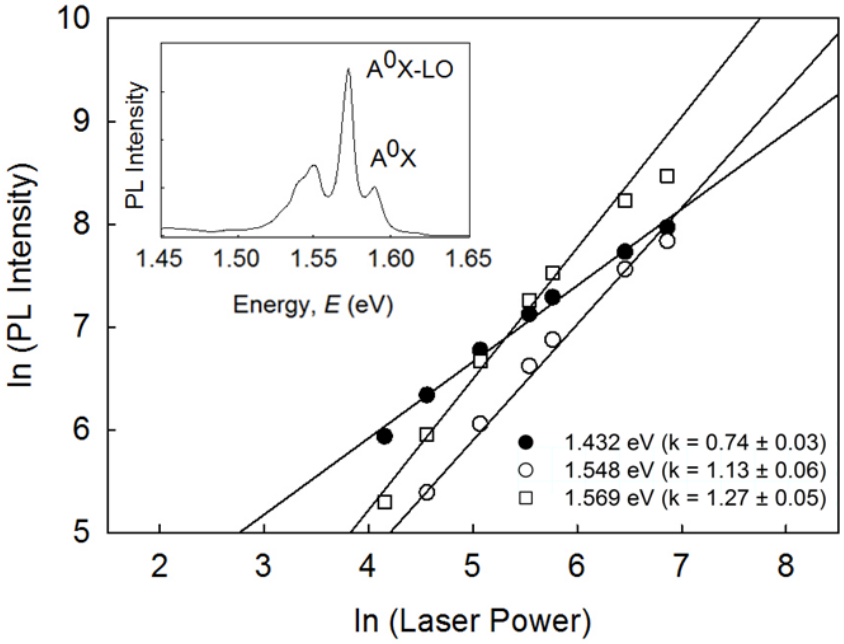

Figure 3: *ln-ln* plot of PL intensity against laser power (the laser power was measured in mW/cm^2) for the 1.569 eV, 1.548 eV (inset) and 1.432 eV (not shown) features of the PL spectra for mechanically removed as-grown NWs. The intensity of PL emission, I was related to the laser power by $I \propto L^k$. Values of $k > 1$ are consistent with excitonic emission, as was seen for the peaks labelled A^0X and A^0X-LO. The peak at 1.428 eV is part of the DAP series.

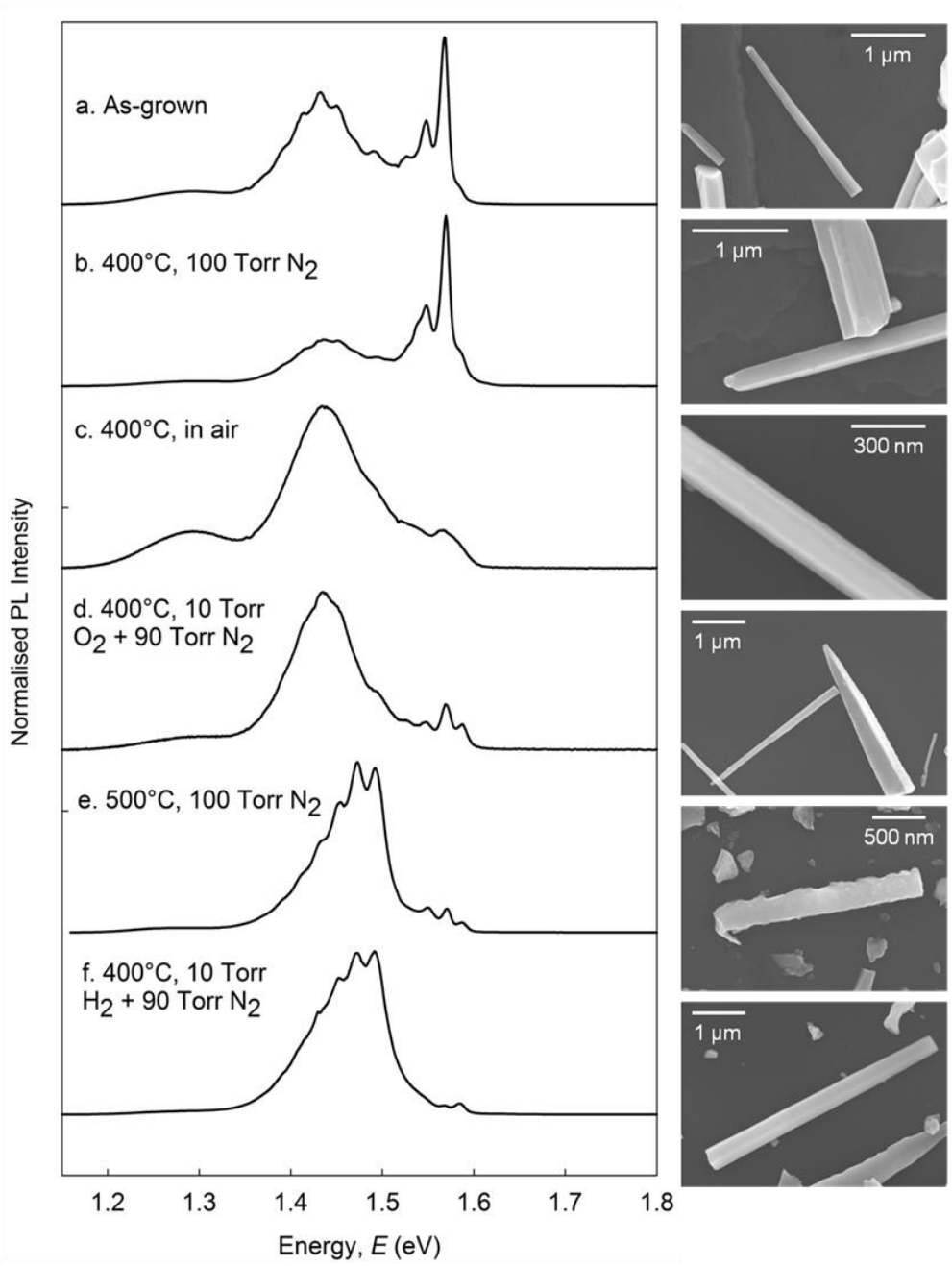

Figure 4: PL spectra of (a) As-grown nanowires and nanowires annealed in (b) 100 Torr N_2 at 400°C (c) air at 400°C, (d) 10 Torr O_2 + 90 Torr N_2 at 400°C, (e) 100 Torr N_2 at 500°C and (f) 10 Torr H_2 + 90 Torr N_2 at 400°C. For all samples, nanowires were mechanically removed onto Si substrates with the spectra being recorded under ~ 60 mW/cm^2 of illumination at 4K. SEM images for each sample are shown to the right of the spectra.

3.3. Post-growth annealing of nanowires.

The results of annealing the wires on both the PL spectra and morphology of the wires as revealed by SEM, are shown in figure 4. The samples are now discussed in three groups, assigned by the character of their PL spectra. Since the number of NWs sampled by the laser beam was not controlled, the intensity of each spectra was normalised by equalising the heights of the highest peaks from spectrum to spectrum, with the relative heights being used for comparative study.

3.3.1. As-grown and annealed in 100 Torr N_2 at 400°C (samples A and B).

Figure 4 shows that the effect of annealing under nitrogen at moderate temperatures was to increase the relative intensity of excitonic over DAP emission, that is to increase the crystal quality of the material. Indeed, by this measure, sample B had the highest quality of all. Presumably the mechanism of improvement is that one of the (electrically active) centres participating in the DAP transition is reduced in concentration by the annealing process. The annealing also introduces a new but weak peak at 1.614 eV, as shown in figure 5. This peak is unusual since it is at higher energy than the band gap energy at 4K, which is 1.605 eV. Since the NWs have diameters in the range 100 – 300 nm, quantum confinement effects are not considered to be responsible. The origins of above-gap emission from CdTe are discussed by Tkachuk [35] and include phonon absorption (LO, TO and TA), excitonic and indirect transitions – a variety of such processes are possible. Tkachuk specifically attributes emission at 1.614 eV to an anti-stokes process involving the free exciton and a TO phonon. Lee *et al.* observed luminescence centred at 1.615 eV (comparable to 1.614 eV in this work) at 4.9K for as-grown *p*-type CdTe, [36], and attributed it to a anti-Stokes process involving an acceptor-bound exciton. As we do not see free exciton emission – at 1.598 eV – we consider the latter to be more probable. For material with strong electron-phonon coupling, as is the case here, a large number of phonons are emitted via the Stokes process making phonons available for absorption even at such low temperatures. Indeed, the Huang-Rhys parameter of the A^0X series for sample B was calculated to be $S = 1.8$, i.e. similar to that for as-grown NWs.

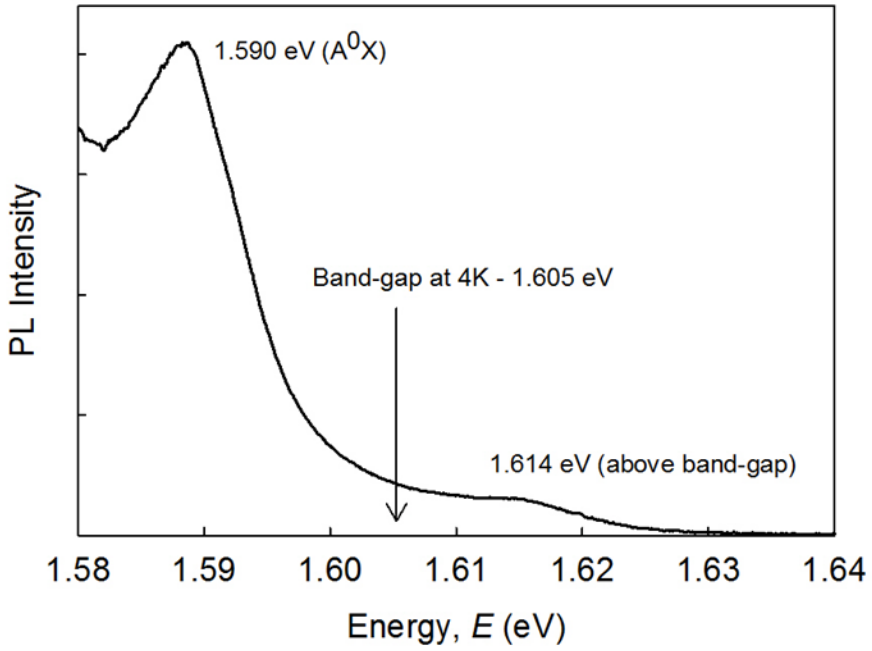

Figure 5: The PL spectrum of sample B - nanowires annealed in 100 Torr N_2 at 400°C – shows evidence of above band-gap luminescence.

3.3.2. Annealing in the presence of oxygen (samples C and D).

Annealing in the presence of oxygen acts to quench the near-edge emission and so the DAP luminescence dominates the normalised spectra. Moreover, the structure of both the near-edge and DAP emission is degraded, with the identity of individual peaks and the appearance of individual phonon replica peaks being lost. Since this effect is greatest for the sample annealed in the greater partial pressure of oxygen (sample C), one may speculate that this is an effect of oxidation. Moreover, the air annealed sample shows a new minor peak at 1.523 eV, and its SEM image shows visible surface change.

3.3.3. Reducing and high temperature annealing conditions (samples E and F)

Annealing at 500°C under N_2 or at 400°C under H_2/N_2 further quenches the near-edge luminescence and enhances the DAP emission. Moreover, the DAP emission changes in character, with the strongest emission now being from the first or second line in the phonon replica series rather than the third. Indeed, the Huang-Rhys coupling parameter is reduced to $S = 0.7$ from its value of 2.5 in the as-grown samples – and this indicates much

reduced electron-phonon coupling in these samples. Even though the transitions are much more weakly coupled to the lattice, the exponents *k* for the first three phonon replicas (see figure 6) are increased only slightly (to 0.82 – 0.84) over their as-grown values of ~ 0.75 – the transitions remain of DAP type even though their character has changed. There is some evidence in the literature that weak phonon coupling is a signature of transitions associated with extended defects or surfaces. Emission at 1.49 eV for example, has been linked to surfaces [37, 38] although not without controversy [39]. Of all the samples A-F examined, only E and F showed visible signs of degradation in the SEM, with roughening of the sidewalls being observed for most of the NWs.

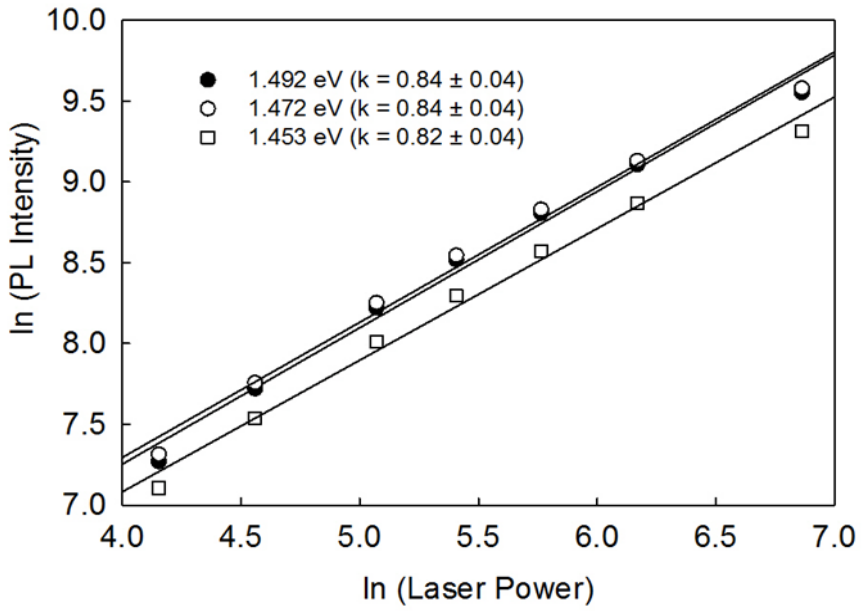

Figure 6: Laser excitation intensity dependence of the PL intensity for three features within the low-energy defect band region (1.4 – 1.5 eV) for sample E – nanowires annealed in 100 Torr N_2 at 500°C.

3.3.4. TEM analysis of as-grown and annealed CdTe nanowires

Extended defects in the II-VI semiconductors are reviewed in Ref. 40 with twinning in CdTe being described in Ref. 4. Since the stacking fault energy of CdTe is relatively low (reported in the range 9 – 10.1 mJ/m^2 [40, 41] the material is particularly prone to stacking faulting, twinning, and the occasional incidence of polytypic stacking sequences.

In order to understand the microstructure of the NWs, ten examples each from samples A and B were imaged in the TEM. It was found that the microstructure was determined only by the growth axis of the NWs, with annealing having no effect on the extended defects. The microstructural trends are therefore now discussed with reference to the growth axis only, with typical examples for each of the growth axes being shown in Figs 7a-d. NWs having one of three growth axes, but no others, were observed, these being <110> (20%), <111> (50%) and <112> (30%). In this work the NWs were grown on a polycrystalline film of sputtered CdTe.

Those growing in the <110> direction (figure 7a) were all defect free, there being no evidence of any planar defects. About 10% of those wires growing with the <111> direction were also defect free (figure 7b), whereas most contained stacking faults inclined at an angle of 70°32' to the growth axis, i.e. on another set of {111} planes, as shown in figure 7c. The highest density of planar faults was seen in those wires growing along the <112> axis, this direction containing a set of {111} planes that extend along the full length of the wires. Twinning, stacking faults and polytypes were observed on these {111} planes. While the twinning and stacking faults often occurred randomly, there was sometimes periodic behaviour, as shown in Fig 7d. The periodicity of the regular structure in the bottom right of the image was consistent with a 4H polytype, that is the stacking sequence AαBβAαCγAαBβAαCγ.

The relationship between the incidence of planar defects and NW growth axis observed in these samples is similar to the trends observed for other low stacking fault energy cubic materials, e.g. Au NWs [42]. For the cases of <110> and <111> oriented wires, the {111} planes (upon which planar defects occur) are all inclined to the growth axis. Hence, whenever they are present, the planar defects soon intersect a NW wall, and they grow out. On the contrary, for <112> oriented growth, the growth axis is contained within a {111} fault plane and hence the planar faults do not grow out but persist along the entire lengths of the wires.

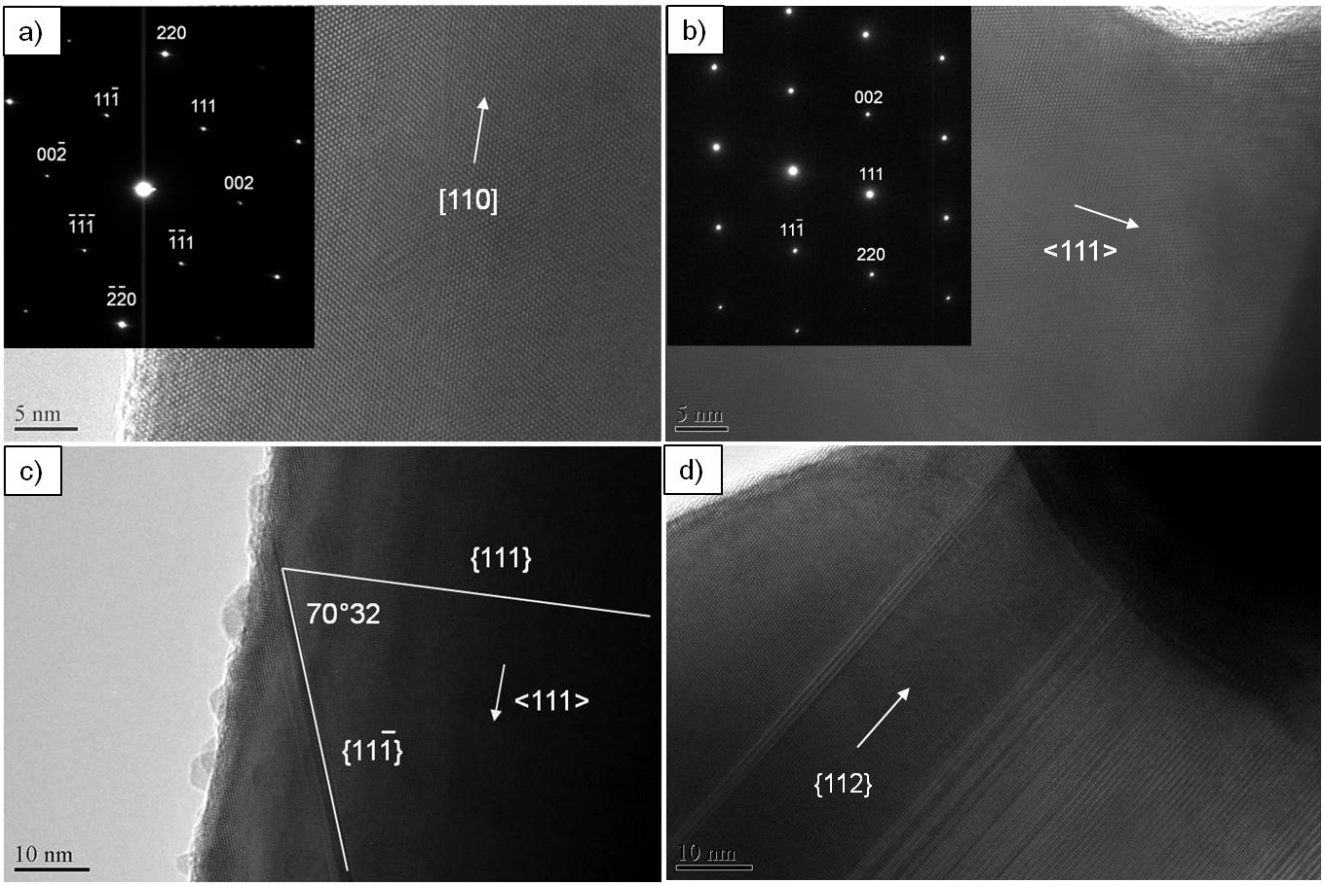

Figure 7: a) Single crystal CdTe NW growing in a [110] direction, free of any planar defects (inset: cubic diffraction pattern). b) Single crystal NW growing in a <111> direction (inset: cubic diffraction pattern). c) A twin in a {111} plane of a NW growing in <111> direction. d) Highly twinned NW growing along a <112> axis. The planar defects persist along the length of <112> wires. This image was taken from close to the catalyst droplet, which is visible in the top right of the micrograph.

4. Conclusions

Au-catalysed CdTe NWs have been grown on polycrystalline CdTe substrates (metamorphic growth) and the defects within them have been evaluated with the aim of assessing their suitability for use in solar PV applications. The influence of post-growth annealing – using steps that are typical for use in PV device processing – has also been evaluated.

Low temperature photoluminescence of the wires shows that they have strong near-band edge features and weak DAP (donor-acceptor-pair) luminescence that is characteristic of single crystal CdTe, rather than the degraded spectra that are normally associated with polycrystalline films. Moreover, annealing under nitrogen at 400°C acts to further improve the crystal quality; that is the relative strength of the near edge compared to DAP emission lines. For the annealed samples, the rarely observed above-gap luminescence was observed, this being attributed to anti-Stokes emission with the participation of an exciton. Such emission is associated with materials having high electron-phonon coupling, which is the case for CdTe. This is supported by the observation of particularly strong phonon coupling to the (A^0X) transition. The dominance of the near-edge emission indicates that the as-grown and annealed wires have sufficiently high optoelectronic quality to make them potentially superior to thin films for PV applications.

Perhaps surprisingly, the spectra did not reveal any exciton band luminescence that could be attributed to the presence of Au (from the catalyst) in the CdTe. Certainly the published accounts of Au acceptor bound exciton luminescence from CdTe:Au show strong lines in positions that could not be confused with the ones observed in this work at the resolution of our experiment. Instead, there were lines that might be attributed to either Ag^0X, Cu^0X or Na^0X, these lines being so close in energy as to be indistinguishable from one another in our experiment. All are possible candidates since they occur as impurities in the Au (Ag and Cu) or the glass (Na). Au however is represented in the spectra by a weak donor-acceptor-pair peak having an intensity maximum of ~1.27 eV. Its presence implies that the deeper levels of Au are optically and perhaps electrically active in these samples.

Annealing of the wires, either at higher temperatures under inert gas (e.g. 500°C under nitrogen) or at lower temperatures under oxidizing or reducing environments caused the degradation of the luminescence by the quenching of the excitonic emission and the dominance of the DAP luminescence. This implies the creation of new populations of point defects that would be deleterious to minority carrier device operation. Such treatments are therefore unlikely to be of value in solar cell device processing.

Extended defects in the wires comprise stacking faults, polytypes and twins only. Annealing did not influence their incidence or type, and they were determined solely by the orientations of the wires. Since they

were grown on polycrystalline underlayers, the wires adopted neither a single growth axis nor a fixed tilt angle with respect to the substrate. Three growth axes dominated and these were <110> at 20% incidence with no planar faults, <111> at 50% incidence with inclined planar faults and <112> at 30% incidence with the highest density of planar faults and lying within the growth axis. For CdTe and other sphalerite semiconductors, these planar defects do not disrupt bonding significantly, and have very little intrinsic electrical activity in pure samples. The recombination activity of these defects is correspondingly low and it may therefore be said that they are not likely to interfere with PV performance in these materials.

Overall, it has been demonstrated that the optoelectronic quality of the Au-catalysed CdTe NWs is generally superior to that of thin films. The NWs do not suffer from the presence of electrically active grain boundaries, and their point defect populations are more similar to those of single crystals than to thin films. Instead, the only defects present are electrically inactive types, and shallow luminescence dominates the PL spectra, this being a positive indication of high crystal quality. However, Au from the catalyst did contribute to deep level emission, and such levels may be deleterious to PV device operation. Since the shallow acceptor lines expected for Au in CdTe were not observed in these materials, further work should include an independent evaluation of the chemical content of Au in the wires. One of the potential advantages of NW PV is the minimization of recombination loss, leading to the possibility to use lower grade starting material. The presence of impurity related deep levels may nevertheless be deleterious to PV device operation, and evaluation of this would require current transport measurement of a junction device (from temperature dependent current transport measurements). If Au-catalysed wires prove unsuitable, then NWs grown with alternative catalysts, such as Sb and Bi, or else self catalysis should be evaluated.

Acknowledgements

The authors acknowledge support of the EPSRC SUPERGEN Initiative for the programme “PV-21”.

References

1. J.R. Sites, J.E. Granata, and J.F. Hiltner, Solar Energy Materials and Solar Cells **55** 43-50 (1998)
2. S.A. Galloway, P.R. Edwards, and K. Durose, Solar Energy Materials and Solar Cells **57** 61-74 (1999)
3. J.D. Major, Y.Y. Proskuryakov, K. Durose, G. Zoppi, and I. Forbes, Solar Energy Materials and Solar Cells **94** 1107-1112 (2010)
4. K. Durose and G.J. Russell, Journal of Crystal Growth **101** 246-250 (1990)
5. H.M. AlAllak, A.W. Brinkman, H. Richter, and D. Bonnet, Journal of Crystal Growth **159** 910-915 (1996)
6. L.O. Bubulac, J. Bajaj, W.E. Tennant, P.R. Newman, and D.S. Lo, Journal of Crystal Growth **86** 536-543 (1988)
7. S.A. Galloway, P.R. Edwards, and K. Durose, in Microscopy of Semiconducting Materials, edited by A.G. Cullis and J.L. Hutchison, Editors., (Iop Publishing Ltd: Bristol,1997). p. 579-582.
8. J. Britt and C. Ferekides, Applied Physics Letters **62** 2851-2852 (1993)
9. M.A. Green, K. Emery, Y. Hishikawa, W. Warta, and E.D. Dunlop, Progress in Photovoltaics **20** 606-614 (2012)
10. M.D. Kelzenberg, S.W. Boettcher, J.A. Petykiewicz, D.B. Turner-Evans, M.C. Putnam, E.L. Warren, J.M. Spurgeon, R.M. Briggs, N.S. Lewis, and H.A. Atwater, Nat Mater **9** 239-244 (2010)
11. L. Tsakalakos, J. Balch, J. Fronheiser, B.A. Korevaar, O. Sulima, and J. Rand, Applied Physics Letters **91** 233117-3 (2007)
12. M.D. Kelzenberg, D.B. Turner-Evans, B.M. Kayes, M.A. Filler, M.C. Putnam, N.S. Lewis, and H.A. Atwater, Nano Letters **8** 710-714 (2008)
13. R. Kapadia, Z. Fang, and A. Javey, Applied Physics Letters **96** id. 103116 (2010)
14. Z. Fan, H. Razavi, J.-w. Do, A. Moriwaki, O. Ergen, Y.-L. Chueh, P.W. Leu, J.C. Ho, T. Takahashi, L.A. Reichertz, S. Neale, K. Yu, M. Wu, J.W. Ager, and A. Javey, Nat Mater **8** 648-653 (2009)
15. B.L. Williams, B. Mendis, L. Bowen, D.P. Halliday, and K. Durose, in MRS Proceedings 1350 (2011) mrss11-1350-ee06-25, doi: 10.1557/opl.2011.872.
16. V.G. Dubrovskii, A. Bolshakov, B.L. Williams, and K. Durose, Nanotechnology **23** 485607 (2012)
17. K. Nakamura, T. Fujihara, T. Toyama, and H. Okamoto, Japanese Journal of Applied Physics Part 1-Regular Papers Short Notes & Review Papers **41** 4474-4480 (2002)
18. G. Zoppi, K. Durose, S.J.C. Irvine, and V. Barrioz, Semiconductor Science and Technology **21** 763-770 (2006)
19. D.R. Wight, D. Bradley, G. Williams, M. Astles, S.J.C. Irvine, and C.A. Jones, Journal of Crystal Growth **59** 323-331 (1982)

20. N.C. Giles-Taylor, R.N. Bicknell, D.K. Blanks, T.H. Myers, and J.F. Schetzina, Journal of Vacuum Science & Technology A: Vacuum, Surfaces, and Films **3** 76-82 (1985)
21. J. Krustok, J. Madasson, K. Hjelt, and H. Collan, Journal of Materials Science **32** 1545-1550 (1997)
22. V. Kosyak, A. Opanasyuk, P.M. Bukivskij, and Y.P. Gnatenko, Journal of Crystal Growth **312** 1726-1730 (2010)
23. P.J. Dean and D.C. Herbert, in Excitons, edited by K. Cho. 1979, Springer: Berlin.
24. T. Schmidt, K. Lischka, and W. Zulehner, Physical Review B **45** 8989-8994 (1992)
25. J. Prochazka, WDS '08 Proceedings of Contributed Papers, Part III 55-60 (2008)
26. W. Shan, W. Walukiewicz, J.W. Ager, K.M. Yu, H.B. Yuan, H.P. Xin, G. Cantwell, and J.J. Song, Applied Physics Letters **86** (2005)
27. C.H. Ahn, S.K. Mohanta, N.E. Lee, and H.K. Cho, Applied Physics Letters **94** (2009)
28. W.K. Hong, G. Jo, M. Choe, T. Lee, J.I. Sohn, and M.E. Welland, Applied Physics Letters **94** (2009)
29. B. Monemar, P.P. Paskov, J.P. Bergman, G. Pozina, A.A. Toropov, T.V. Shubina, T. Malinauskas, and A. Usui, Physical Review B **82** (2010)
30. N. Magnea, in Properties of Narrow Gap Cadmium-Based Compounds, edited by P. Capper (INSPEC, Exeter, 1995)
31. E. Molva, J.L. Pautrat, K. Saminadayar, G. Milchberg, and N. Magnea, Physical Review B **30** 3344-3354 (1984)
32. J. Hamann, A. Burchard, M. Deicher, T. Filz, V. Ostheimer, F. Strasser, H. Wolf, and T. Wichert, Physica B-Condensed Matter **273-4** 870-874 (1999)
33. D. de Nobel, Philips Res. Rep. **14** 361 (1959)
34. S. Vatavu, H. Zhao, V. Padma, R. Rudaraju, D.L. Morel, P. GaÅŸin, I. Caraman, and C.S. Ferekides, Thin Solid Films **515** 6107-6111 (2007)
35. P.N. Tkachuk, V.I. Tkachuk, N.D. Korbutjak, A.N. Raransky, D.V. Korbutyak, and S.G. Krylyuk, Journal of Crystal Growth **184** 536-540 (1998)
36. J. Lee, N.C. Giles, and C.J. Summers, Physical Review B **49** 11459-11462 (1994)
37. H.-X. Han, B.J. Feldman, M.L. Wroge, D.J. Leopold, and J.M. Ballingall, Journal of Applied Physics **61** 2670-2671 (1987)
38. R. Ahmad-Bitar, H. Moutinho, F. Abulfotuh, and L. Kazmerski, Renewable Energy **6** 553-558 (2005)
39. H.L. Cotal, A.C. Lewandowski, B.G. Markey, S.W.S. McKeever, E. Cantwell, and J. Aldridge, Journal of Applied Physics **67** 975-982 (1990)
40. S. Takeuchi, K. Suzuki, K. Maeda, and H. Iwanaga, Philosophical Magazine a-Physics of Condensed Matter Structure Defects and Mechanical Properties **50** 171-178 (1984)

41. G. Lu and D.J.H. Cockayne, Philosophical Magazine a-Physics of Condensed Matter Structure Defects and Mechanical Properties **53** 307-320 (1986)
42. J. Wang, M. Tian, T.E. Mallouk, and M.H.W. Chan, The Journal of Physical Chemistry B **108** 841-845 (2003)